Mem. S.A.It. Vol. 94, 17

Memorie della

Stellar probes of dark matter

Raghuveer Garani

INFN Sezione di Firenze, Via G. Sansone 1, I-50019 Sesto Fiorentino, Italy.
e-mail: garani@fi.infn.it

Received: 08-02-2023; Accepted: 17-04-2023

Abstract. Celestial bodies are efficient probes to unveil interactions between standard model and dark matter (DM) particles. From elastic scatterings on stellar matter, DM can get gravitationally trapped by the body. Annihilation of accumulated DM particles can result in novel and observable effects that can constrain DM scattering cross section with the visible sector. In this talk I will illustrate the constraining power of terrestrial and space borne experiments to such scenarios. DM annihilation in compact objects such as old ideal neutron stars (NS) can heat them up to temperatures of 2600 K. Black body spectrum of such warm NS peak at near infrared wavelengths with magnitudes in the range potentially detectable by the James Webb Space Telescope (JWST). I will demonstrate that NS with surface temperatures > 2400 K, located at a distance of 10 pc can be detected by the NIRCAM instrument at SNR > 10 within 24 hours of exposure time. Observation of such NS would constrain DM elastic scattering cross section $\sim 10^{-45}$ cm^2.

1. Introduction

Compact stellar objects such as neutron stars (NS) offer a unique playground to probe not only the physics of high density nuclear matter but also several beyond the standard model possibilities. Many of these are pictorially shown in the cartoon Fig. 1.

This talk is based on the recent works Chatterjee et al. ; Garani and Heeck ; Garani et al. , and contains three parts. The first part reviews our current understanding of neutron star properties such as mass and radius. The second part shows how the properties of light particles such as axions (and other long range force carriers) could be constrained through observations of pulsars, and through gravitational waves emitted from binary neutron star mergers. The final part, while being speculative, examines the possibility of observing dark matter (DM) heated old neutron stars in the local bubble. Such observations can constrain DM interactions with visible matter $\sim 10^{-45}$ cm^2.

Fig. 1. Cartoon illustrating several phenomena that could be probed through celestial bodies such as neutron stars.

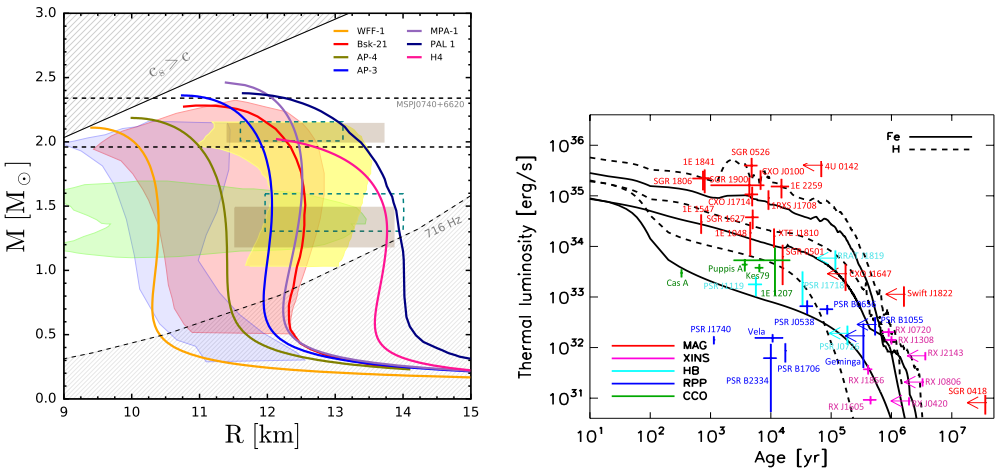

Fig. 2. *Left panel:* Mass-radius relation for representative EoS for nuclear matter at high densities, reproduced from Özel and Freire ; Chatterjee et al. . The blue shaded area indicates preferred region from observation of pulsars Özel and Freire . The yellow region is preferred by the observation of binary NS merger where the fit was performed for purely hadronic EoS. The green region indicates the 90% CL obtained from EoS insensitive fit from GW170817 Abbot et al. . Bayesian fits at 90% CL from combination of gravitational wave data and low energy nuclear and astrophysical data are shown as red regions. The horizontal thick-dashed lines show the mass measurement of the heaviest observed pulsar MSP J0740+6620 of $2.14^{+0.2}_{-0.18}$ $M_\odot$ at 95% CL. The dashed curve labelled 716 Hz represents the limit on the M-R of the fastest spinning pulsar obtained using observations from the Green Bank Telescope. *Right panel:* Reproduced from Vigano et al. , depicts magneto-thermal evolution of isolated NS. A comparison between observational data and theoretical cooling curves, for two representative models with magnetic fields 0, 3×10^{14}, 3×10^{15} G are shown, for Fe envelopes (solid) and light-element envelopes (dashed)

2. NS so far

In the left panel of fig. 2, we show the mass-radius relationship for NS composed predominantly of neutrons ($\sim$ 90%) and proton+lepton ($\sim$ 10%) matter. The multi-colored curves in this figure correspond to different assumptions of micro-physics and computational techniques, and are compiled in Özel and Freire . The shaded regions display the M-R values supported by various observations and experiments. The green shaded area show 90% confidence limits obtained by performing a fit for the tidal deformability and mass using EoS-insensitive methods from recent gravitational wave observations of mergers of binary NS Abbot et al. . Tidal deformability data fit to purely hadronic EoS using the latest outer core model results in yellow shaded regions at 3-σ. Bayesian fits obtained by combining gravitational wave data with low energy nuclear and astrophysical data are shown as red regions at 90% confidence level. Radio and X-ray observation of pulsars Özel and Freire are shown by light blue area. Simultaneous mass-radius measurements of PSR J0030+0451 and J0740+6620 by NICER Riley et al. ; Miller et al. are shown as green dashed and brown shaded rectangular regions representing 68% confidence limits, respectively.

In the right panel of fig. 2, magneto-thermal evolution of NS are shown Vigano et al. . Having also explored the influence of their initial magnetic field strength and geometry, their mass, envelope composition, and relevant microphysical parameters such as the impurity content of the innermost part of the crust (the pasta region), thermodynamic evolution curves were derived. The curves closely follow those

of minimal cooling or passive cooling models. The figure clearly shows that cold and old isolated NSs have remained so far unobserved. The coldest NS observed have surface temperatures $\sim 4 \times 10^4$ K, while the age remains uncertain. With current data, theoretical models of late evolutionary stages of NS has not been tested. As we will show here, JWST can in principle shed light on these aspects of NS physics.

3. Axion and other searches

Any new light degree of freedom that couple to nucleons, such as axions, would contribute to cooling of NS by opening up additional emission channels. For example, by noting the observation of hot neutron star in the supernova remanant HESS J1731-347 stringent constraints are derived on very light axions $\lesssim$ keV Beznogov et al. . A limit on the axion decay constant $> 10^9$ GeV was obtained. There have been several works in this direction. Most existing limits were compiled O'Hare and are readily available on the website https://cajohare.github.io/AxionLimits/.

Recent observation of gravitational waves (GWs) from binary NS mergers can also be used to place stringent constraints on new long range force carriers. This was shown in Poddar et al. ; Dror et al. , where strong limits ($g'_{\mu-\tau} < 10^{-20}$) on fifth force carriers that couples to only second-third generation of leptons were obtained, for masses below $O(10^{-10})$ eV.

4. WIMP dark matter searches: heating

The maximum rate at which DM particles can be gravitationally captured by any celestial body solely depends on their mass (M), radius (R), velocity ($v_\star$), the DM dispersion velocity (v_d) and the ambient DM density (ρ_χ). This is often referred to as the geometric capture limit. This is considered for the capture rate when the DM mean free path is approximately smaller than the object's radius, corresponding to DM scattering cross section $\sigma \gtrsim \sigma^{\rm g}_\star$ Goldman and Nussinov ; Tinyakov et al.. Typically, NS are dense objects with escape velocities (v_{esc}) being much larger than other velocity scales in the capture process. For a given DM mass (m_χ), the maximum capture rate (geometric rate) is given by

$$C^{\rm g}_\star = \pi R^2 \frac{\rho_\chi}{m_\chi} \frac{\langle v\rangle_0}{1-v^2_{esc}} \sqrt{\frac{3\pi}{8}} \frac{v^2_{esc}}{v_\star v_d} \,{\rm Erf}\left(\sqrt{\frac{3}{2}}\frac{v_\star}{v_d}\right),$$

with $\langle v\rangle_0 = \sqrt{8/(3\pi)} v_d$, the escape velocity $v_{esc} = \sqrt{2GM/R}$ from the neutron star, and the error function is denoted by Erf. This expression is valid in the limit $v_{esc} \gg v_\star, v_d$. Thus the accretion rate strongly depends on the EoS of the neutron star through v_{esc}, and modestly on variables ρ_χ, $v_\star$ and v_d. When the DM mean free path is approximately larger than the NS radius, the geometric capture rate above should be rescaled by factor $\sigma/\sigma^{\rm g}_\star$. One of the main goal of this discussion is to systematically evaluate how the maximum capture rate in the single scattering regime, and consequently, the maximal neutron star heating induced by DM capture and annihilation and the prospect of their detection at JWST.

DM particles in the halo are accelerated to semi-relativistic velocities as it impinges on the NS. Scattering of the DM particles with particles in the stellar medium (n, p, μ, e) can result in the capture of DM in NS as most of their initial kinetic energy is deposited to NS medium, thereby heating it up Baryakhtar et al. . Next, if DM particles can annihilate during the current cosmological epoch, the accumulated DM in the core of NS would also annihilate upon thermalization with NS medium Garani et al. . Further heating of the NS is possible, if the products of annihilation process deposit all their energy in the NS medium. In this case, the total energy deposited is equal to the sum of kinetic and annihilation energies, dubbed here as KA heating. The kinetic and annihilation energies deposited are $m_\chi(\gamma-1)C^{\rm g}_\star$ and $m_\chi C^{\rm g}_\star$, respectively. Here, $\gamma = (1-2GM/R)^{-1/2}$ is the gravitational redshift factor. Therefore, the deposited energies are independent of DM mass. Note, however, there exists a lower limit on the DM mass below which DM evaporation

from the NS dominates. This lower limit is set when the ratio of escape energy from the core to the core temperature is $\sim$ 30 Garani and Palomares-Ruiz . For isolated and cold NS, the kinetic only, or the KA energy can effectively render the NS observable by increasing the surface temperature which translates directly to the luminosity, as given by the Stefan-Boltzmann law ($4\pi R^2 \sigma_{\rm B} T_{\rm eff}^4$). For an observer far away from the NS, the apparent temperature is $T^\infty = T_{\rm eff}/\gamma$. The contributions from kinetic only, and KA heating can be computed as

$$T^\infty_{\rm kin} \approx 1787\,{\rm K}\left[\frac{\alpha_{\rm kin}}{0.08}\left(\frac{\rho_\chi}{0.42\,{\rm GeV/cm^3}}\right)\times\left(\frac{220\,{\rm km/s}}{v_\star}\right){\rm Erf}\left(\frac{270\,{\rm km/s}}{v_d}\frac{v_\star}{220\,{\rm km/s}}\right)\right]^{1/4},$$

$$T^\infty_{\rm KA} \approx 2518\,{\rm K}\left[\frac{\alpha_{\rm KA}}{0.33}\left(\frac{\rho_\chi}{0.42\,{\rm GeV/cm^3}}\right)\times\left(\frac{220\,{\rm km/s}}{v_\star}\right){\rm Erf}\left(\frac{270\,{\rm km/s}}{v_d}\frac{v_\star}{220\,{\rm km/s}}\right)\right]^{1/4},$$

with,

$$\alpha_{\rm kin} = \frac{(\gamma-1)(\gamma^2-1)}{\gamma^4}, \alpha_{\rm KA} = \frac{\gamma(\gamma^2-1)}{\gamma^4}\,. \quad (1)$$

The above expressions are normalized to $M = 1.5\,M_\odot$ and $R = 10$ km. Note that $\alpha_{\rm KA}$ ($\alpha_{\rm kin}$) is maximized for $\gamma = 1.732\,(2.56)$.

Caveats.–Mechanisms of kinetic and KA heating can heat the NS up to $O(10^3)$ K after about 100 Myrs. However, for similar ages, other mechanisms of heating can begin to work, if exotic phases such as neutron/proton superfluidity are realized in their cores. Generically, heat can be injected into the NS by conversion of magnetic, rotational, and/or chemical energies Özel and Freire . In such scenarios, the intrinsic heating signature is degenerate with that of DM heating, challenging its interpretation. Constraints on DM parameter space can nevertheless be placed if NS with effective surface temperature $\lesssim 2\times10^3$ K were to be observed Hamaguchi et al. .

5. Searches with JWST

We now compute the luminosities of NS from DM accretion heating. For each set of (M, R) given by EoS i we compute the DM geometric capture rate averaging over DM phase space parameters through $C^{\rm g}_{i,j}(M,R) = \kappa\sum_{k,l}\int dv_\star p_j(v_\star) C^{\rm g}_\star(i, v_\star, v_d^k, \rho_\chi^l)$, where, $j = 1, 5$ corresponds to the different velocity probability distributions (p_j) of NS (see Chatterjee et al. for further details), and the averaging coefficient $\kappa = (k_{\rm max}\, l_{\rm max})^{-1}$. Integers $k_{\rm max}$(=2) and $l_{\rm max}$(=2) denote the number of values we sample for parameters v_d and ρ_χ, respectively. When both kinetic and annihilation heating processes are operative, the effective surface temperature $T^\infty_{i,j}$ is obtained by summing both contributions $(m_\chi(\gamma-1)+m_\chi)C^g_{i,j}$ and equating it to the apparent luminosity. Next, we average over the NS velocity distributions by $\langle C^g_i\rangle = \sum_j C^g_{i,j}/j_{\rm max}$ to get an effective average surface temperature $T^\infty_{{\rm avg},i}$. Assuming the NS to be a black body, we compute the spectral energy distribution (SED) as follows

$$f_\lambda(M,R) = \frac{4\pi^2}{\lambda^3}\left(e^{\frac{2\pi}{\lambda T^\infty}}-1\right)^{-1}\left(\frac{R\gamma}{d}\right)^2\,. \quad (2)$$

Here R and d are the radius (typically 10 km) and distance (taken to be d=10 pc) to the NS, and the factor $R\gamma/d$ is the angle subtended by the NS to the observer. The flux density at a given wavelength λ is denoted by $f_\lambda(M,R)$, and T^∞ is the surface temperature of the NS. In Fig. 3 (left panel), we display the SEDs due to KA heating, encompassing the temperature range for each combination of mass and radius considered here, and other astrophysical parameters discussed in ref. Chatterjee et al. . The maximal difference in the temperature between the MAX and MIN scenario is $\sim$ 40%.

As evident from Fig. 3 (left panel), the SEDs peak at $\lambda \sim 2\,\mu$m in the near-infrared bands with maximum flux values $\sim$ 2.5 nJy. Owing to the compact ($R \sim 10$ km) size of NS, they will appear as unresolved, extremely faint point sources, even for a cutting-edge facility such as the JWST. In the right panel of Fig. 3, we demonstrate the sensitivity of the Near-Infrared Camera (NIRCAM) on the

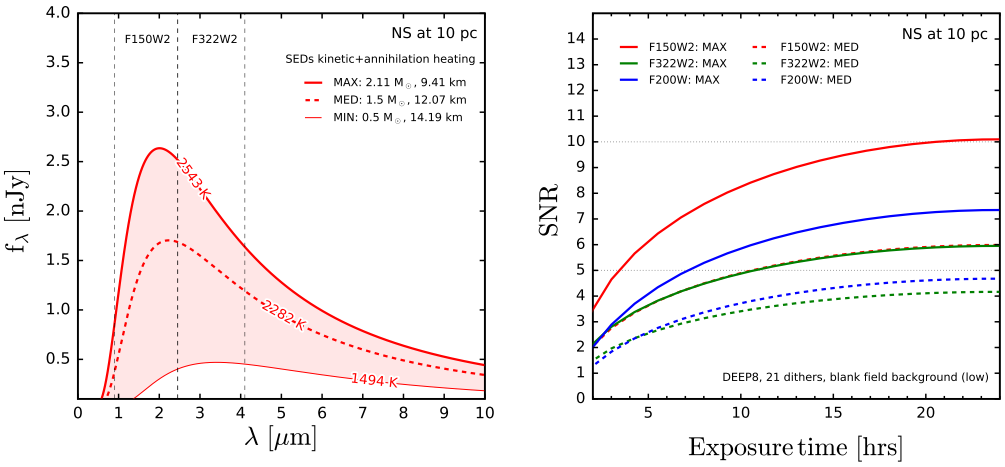

Fig. 3. *Left panel:* Range of black body spectral energy distributions for the case of kinetic+annihilation heating, for old isolated NS at 10 pc are shown in red. The thick solid line, dashed line, thin line, correspond to effective temperatures of 2543 K, 2282 K, 1494 K, and mass (radius) of $M = 2.11\,M_\odot$ (9.41 km), $M = 1.5\,M_\odot$ (12.07 km), $M = 0.5\,M_\odot$ (14.19 km), respectively. Dashed lines were obtained upon averaging over all EoS independent inputs, while the solid (thin) line is representative of the maximum (minimum) value of effective temperature over all EoS we consider over the mass range $0.5 - 2.2\,M_\odot$. Vertical dashed lines delimit the bandwidth of filters F150W2 and F322W2. *Right panel:* The signal-to-noise ratio (SNR) is shown as a function of exposure time for filters F150W2 and F322W2, and narrow band filter F200W.

JWST, to the MAX, and MED, SEDs shown in the left panel. The signal-to-noise ratio (SNR) is plotted as a function of the exposure time, where the SNR is computed using the exposure time calculator (ETC) specifically dedicated for JWST and WFIRST missions. The SEDs displayed in Fig. 3 (left) are injected to the ETC as source flux distributions. With the use of JWST background tools we generate a reference (low) background model for a blank field given by coordinates RA='03 32 42.397' and Dec= '-27 42 7.93'. NIRCAM offers only two very wide-band filters, that allow for effective collection of large amounts of photons. They are F150W2 and F322W2, roughly corresponding to the near-infrared H and L bands, and their wavelength coverage is marked in Fig. 3 (left) using vertical dashed lines. The very faint nature of the targets require the DEEP8 readout pattern in order to minimize data volume. Given that this readout pattern will be strongly affected by cosmic-rays, we have assumed 21 dithers. From this figure, it is seen that NS with maximal KA heating (MAX) has excellent prospects to be detected at SNR $\sim$ 5–10 in <24 hrs of observing time with F150W2. While the prospects for the MIN and kinetic heating only scenarios are poor at JWST. Detecting MED scenario is possible only at a SNR$\sim$ 5 after 24 hrs of exposure (25hr limit for a JWST small program) for the filter F150W2. Assuming a reference (high) background reduces the maximum attainable SNR within a day of observation by at most three units.

6. Conclusions

In this *talk*, I have *quantified* the observational prospects for maximum DM heating scenario of NS, corresponding to geometric values of scattering cross section $\sim 10^{-45}$ cm^2. The effective surface temperature of NS due to DM heating depends on the NS mass and radius through the EoS, the NS velocity in the local bubble, DM velocity and number density. The corresponding variations of the NS effective surface temperature are shown in Fig. 3,

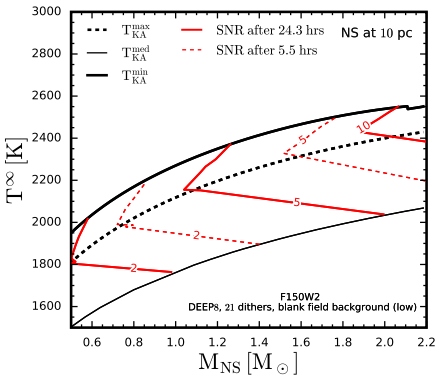

Fig. 4. The effective temperature due to kinetic+annihilation heating, for old isolated NS at 10 pc, is shown as a function of its mass. The black solid thick (thin) curves are the maximum (minimum) possible temperature obtained upon averaging over astrophysical parameters. The contours of SNR corresponding to exposure time of 24.3 (5.5) hrs, for the filter F150W2 are shown in red solid (dashed) lines. The readout mode, reference background model and the number of dithers are the same as in Fig. 3

and have been assessed together with its impact on the observability of such NS using the NIRCAM instrument on the JWST. As shown in Fig. 4 NS warmer than $\gtrsim 2600$ K, in the local bubble, are observable with strategies requiring exposure times smaller than 24 hrs. These scenarios can be realized in a particle physics model dependent way, or due to internal heating mechanisms independent of DM Hamaguchi et al. . Observation of such NS would not only shed light on late evolutionary stages, but also on their equation of state.

Acknowledgements. R.G. is supported by MIUR grant PRIN 2017FMJFMW and acknowledges partial support from the Spanish MCIN/AEI/10.13039/501100011033 grant PID2020-113334GB-I00.

References

S. Chatterjee, R. Garani, R. K. Jain, B. Kanodia, M. S. N. Kumar and S. K. Vempati, [arXiv:2205.05048 [astro-ph.HE]].
R. Garani and J. Heeck, Phys. Rev. D **100** (2019) no.3, 035039
R. Garani, Y. Genolini and T. Hambye, JCAP **05** (2019), 035
F. Özel and P. Freire, Ann. Rev. Astron. Astrophys. **54** (2016), 401-440
B. P. Abbott *et al.* [LIGO Scientific and Virgo], Phys. Rev. Lett. **121** (2018) no.16, 161101
T. E. Riley, A. L. Watts, S. Bogdanov, P. S. Ray, R. M. Ludlam, S. Guillot, Z. Arzoumanian, C. L. Baker, A. V. Bilous and D. Chakrabarty, *et al.* Astrophys. J. Lett. **887** (2019) no.1, L21
M. C. Miller, F. K. Lamb, A. J. Dittmann, S. Bogdanov, Z. Arzoumanian, K. C. Gendreau, S. Guillot, W. C. G. Ho, J. M. Lattimer and M. Loewenstein, *et al.* Astrophys. J. Lett. **918** (2021) no.2, L28
D. Viganò, N. Rea, J. A. Pons, R. Perna, D. N. Aguilera and J. A. Miralles, Mon. Not. Roy. Astron. Soc. **434** (2013), 123
M. V. Beznogov, E. Rrapaj, D. Page and S. Reddy, Phys. Rev. C **98** (2018) no.3, 035802
Ciaran O'Hare, doi:10.5281/zenodo.3932430
J. A. Dror, R. Laha and T. Opferkuch, Phys. Rev. D **102** (2020) no.2, 023005
T. Kumar Poddar, S. Mohanty and S. Jana, Phys. Rev. D **100** (2019) no.12, 123023
I. Goldman and S. Nussinov, Phys. Rev. D **40** (1989), 3221-3230
P. Tinyakov, M. Pshirkov and S. Popov, Universe **7** (2021) no.11, 401
M. Baryakhtar, J. Bramante, S. W. Li, T. Linden and N. Raj, Phys. Rev. Lett. **119** (2017) no.13, 131801
R. Garani, A. Gupta and N. Raj, Phys. Rev. D **103** (2021) no.4, 043019
R. Garani and S. Palomares-Ruiz, JCAP **05** (2022) no.05, 042
K. Hamaguchi, N. Nagata and K. Yanagi, Phys. Lett. B **795** (2019), 484-489